

Dislocation nucleation in bcc Ta single crystals studied by nanoindentation

Monika M. Biener, Juergen Biener,* Andrea M. Hodge, and Alex V. Hamza

*Nanoscale Synthesis and Characterization Laboratory, Lawrence Livermore National Laboratory, P.O. Box 808,
L-367 Livermore, California 94550, USA*

(Received 24 July 2007; published 18 October 2007)

The study of dislocation nucleation in close-packed metals by nanoindentation has recently attracted much interest. Here, we address the peculiarities of the incipient plasticity in body centered cubic (bcc) metals using low index Ta single crystals as a model system. The combination of nanoindentation with high-resolution atomic force microscopy provides us with experimental atomic-scale information on the process of dislocation nucleation and multiplication. Our results reveal a unique deformation behavior of bcc Ta at the onset of plasticity, which is distinctly different from that of close-packed metals. Most noticeably, we observe only one rather than a sequence of discontinuities in the load-displacement curves. This and other differences are discussed in the context of the characteristic plastic deformation behavior of bcc metals.

DOI: [10.1103/PhysRevB.76.165422](https://doi.org/10.1103/PhysRevB.76.165422)

PACS number(s): 62.20.Fe, 63.10.+a

I. INTRODUCTION

Nanoindentation has become a valuable tool in the study of fundamental aspects of plasticity such as dislocation nucleation.¹⁻⁷ The power of this technique lies in its ability to probe ultrasmall and therefore virtually defect-free sample volumes. In the case of carefully prepared single crystal metal surfaces, the onset of plasticity in nanoindentation experiments is typically marked by a more or less pronounced discontinuity in the load-displacement curves.^{3,8,9} These so-called “pop-ins” are generally explained by homogeneous dislocation nucleation, which is consistent with the observation that pop-ins typically occur when the resolved shear stress under the indenter approaches the theoretical shear strength of the material under investigation.

The goal of the present work is to advance our understanding of incipient plasticity in body centered cubic (bcc) systems. Compared to face centered cubic (fcc) systems, the plastic behavior of bcc metals is very complex and is still relatively poorly understood.¹⁰⁻¹⁴ As a consequence, only a few nanoindentation studies have addressed dislocation nucleation in pure bcc single crystals.¹⁵⁻²¹ Most of these studies have been performed on Fe-3 wt % Si and W and report pop-in events which are distinctly different from those observed on close-packed metals: Typically, only one large pop-in event is observed in contrast to the multiple pop-in, staircaselike behavior of close-packed metals.^{15,16,18,21} Surprisingly, instead of discussing this difference in the context of the crystal structure, large pop-ins in bcc metals have been linked to oxide rupture.^{15,22} Although oxide rupture may indeed control the yielding behavior in the presence of a thick oxide film, our results will show that this is not true for a system covered with a 1-nm-thick native oxide film.

Here, we analyze the incipient plasticity of bcc, low index Ta single crystals with an emphasis on Ta(001) at the atomic scale. Employing high-resolution atomic force microscopy (AFM) allows us to correlate pop-in events with the appearance of dislocation traces. Our observations are consistent with the idea that the occurrence of a pop-in marks the onset of dislocation activity rather than oxide rupture. We discuss the differences of fcc and bcc systems with respect to the

pop-in behavior in the context of the crystal structure and the consequences thereof. The effect of surface roughness on the pop-in behavior is addressed by modifying the surface roughness by means of ion bombardment in a controlled fashion. These experiments reveal the importance of heterogeneous dislocation nucleation.

Tantalum was selected for the following reasons: (1) Its high melting temperature (3290 K) allows us to study the bcc peculiarities at room temperature (bcc metals typically show a transition between bcc-type and fcc-type behaviors at $0.15 T_{\text{melting}}$ (Ref. 13)); (2) Ta has a very thin and stable native oxide layer (~ 1 nm); (Ref. 23) (3) the mechanical behavior of Ta at the macroscale has been well studied; (Ref. 24–29); and (4) tantalum is a very interesting engineering material due to its high density, high fracture toughness and ductility, and corrosion resistance.

II. EXPERIMENT

The Ta single crystals (Surface Preparation Laboratory) used in the current study were prepared by a combination of electrochemical and mechanical polishing, resulting in a rms surface roughness well below 1 nm. Both in-plane and out-of-plane surface orientations were determined by electron backscatter diffraction (EBSD). The thickness of the native oxide layer was verified by sputter depth profiling using x-ray photoelectron spectroscopy, and the sputter rate was calibrated to a standard Ta₂O₅ sample. All nanoindentation experiments (Triboindenter, Hysitron) were performed in the load-controlled mode at loading rates between 50 and 5000 $\mu\text{N/s}$. A Berkovich tip with a radius of curvature of ~ 190 nm was used to obtain quantitative load-displacement data, and a spherical tip with a tip radius of ~ 1 μm was employed to study the material flow under the indenter. The indent morphology was analyzed by contact mode AFM (Molecular Imaging) using ultrasharp tips from Nanosensors.

III. RESULTS AND DISCUSSION

A. Nanoindentation

The onset of plasticity in Ta(001) during nanoindentation is marked by a pronounced discontinuity [Fig. 1(a)]. The

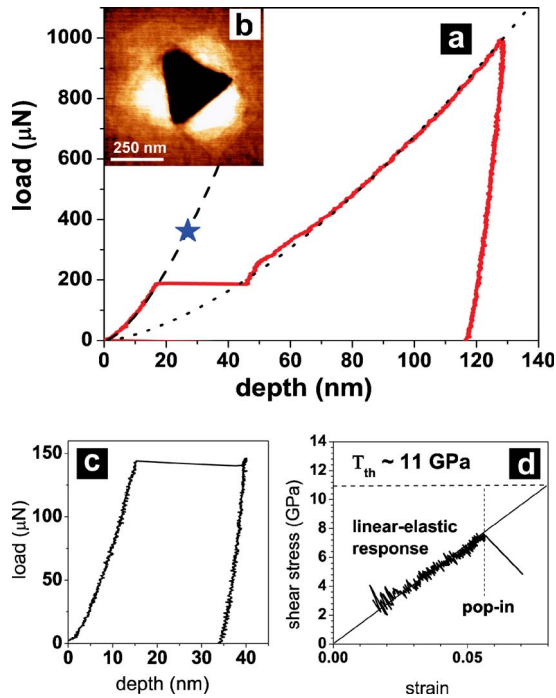


FIG. 1. (Color online) Nanoindentation tests performed on a Ta(001) single crystal surface using a Berkovich tip: (a) a typical load-displacement (P - h) curve with a pronounced discontinuity marking the onset of plasticity. The dashed line is a fit of the initial elastic loading section to the Hertzian contact law. The star symbol marks the condition where the maximum resolved shear stress reaches the theoretical shear stress of Ta. The elastic-plastic part of the P - h curve is fitted to the Taylor dislocation model (dotted line) (Ref. 33). A P - h curve (c) and corresponding AFM image (b) from a test loaded just above the onset of plasticity. (d) Maximum resolved shear stress versus representative strain plot of the nanoindentation data shown in (c). Note the linear elastic response up to a strain of 0.055.

displacement excursion is typically around 30 nm in depth, which suggests that at least 100 dislocations (the Burgers vector of Ta is 0.286 nm) are generated on the time scale of the pop-in (~ 1 ms) and contribute to the observed displacement burst. This observation points toward a very efficient dislocation multiplication process in bcc materials in the complex stress field under the indenter. Once plasticity starts, the material flows continuously, which means that no further pop-ins are observed. Deformation in the subcritical load regime is fully elastic and unloading leads to a full recovery, as confirmed by AFM.³⁰ The load-displacement behavior as described above is very reproducible, and we observe a narrow distribution of the critical load necessary to initiate plasticity [see also Fig. 3(a)].

The elastic portion of the P - h curve can be fitted by the Hertzian contact theory,³¹

$$P = 4/3E_r R^{1/2} h^{3/2},$$

where R is the radius of the blunted Berkovich tip and E_r is the reduced modulus of the tip-sample system. An excellent agreement between experiment and theory is obtained by

assuming a tip radius of 190 nm [Fig. 1(a), dashed line]. To describe the elastic-plastic part of the P - h curve, we follow the Taylor relation-based approach developed by Nix and Gao,³² Qiu *et al.*,³³ and Durst *et al.*²¹ In short, the load-displacement (P - h) relationship in the elastic-plastic regime can be expressed by $P = A_c C \sigma$ where $A_c = 24.5h^2$ is the contact area of the Berkovich tip and C is the constraint factor. The stress σ is controlled by two terms, the internal friction stress σ_{friction} (large for bcc metals) and the Taylor stress σ_{Taylor} , which accounts for dislocation interactions, $\sigma = \sigma_{\text{friction}} + \sigma_{\text{Taylor}}$. The latter term is described by the Taylor relation: $\sigma_{\text{Taylor}} = M \alpha G b \sqrt{\rho}$, where M is the Taylor factor, α is an empirical factor, G is the shear modulus, and b is the magnitude of the Burgers vector. The dislocation density ρ is a function of depth and is a linear superposition of the intrinsic dislocation density ρ_s and the density of geometrically necessary dislocations ρ_{GND} . According to a model developed by Nix, the density of the geometrical necessary dislocations can be expressed by

$$\rho_{\text{GND}} = 1.5f^{-3} \tan^2 \theta (bh)^{-1},$$

where θ is the angle between the surface and the indenter, and f is a correction factor introduced by Durst *et al.*²¹ to account for a more realistic deformation volume. Here, we use the following parameter values: $C = 3$, $M = 3$, $\alpha = 0.5$, $G = 69$ GPa, $b = 0.286$ nm, $f = 2.6$, and $\theta = 20^\circ$. Specifically, we obtain an excellent fit to our experimental P - h curves over the entire load range (200 μN –9 mN) by assuming a friction stress of 100 MPa and an intrinsic dislocation density of 10^{12} m^{-2} [Fig. 1(a), dotted line]. The latter value is consistent with a high-quality single crystal and implies that we are indeed able to probe virtually defect-free materials in our experiment. The high value of the intrinsic lattice resistance is a typical property of bcc metals and strongly affects the load-displacement behavior, as discussed below.

To study the details of the elastic-plastic transition, we performed a number of experiments around the critical load. Such a data set is shown in Fig. 1(c) and the corresponding AFM image is displayed in Fig. 1(b). Even right after the pop-in, we observe fine slip lines around the indent, revealing dislocation activity [see also the AFM image shown in Fig. 4(a)]. We never observed any indication for cracking or oxide rupture. In the context of dislocation nucleation, it is useful to convert the original P - h data into physically more meaningful stress-strain data. For a spherical indenter, the maximum resolved shear stress τ_{max} is connected to the mean contact pressure p_{mean} by $\tau_{\text{max}} \sim 0.465 p_{\text{mean}}$.³⁴ Here, p_{mean} is given by $P/\pi a_c^2$, where a_c is the contact radius at load P . The representative strain ε under a spherical indenter in the elastic regime is given by the relationship $\varepsilon = 0.2 (\delta/R)^{-1/2}$, where δ is the indenter displacement and R is the tip radius.^{35,36} The result of such a stress-strain conversion is shown in Fig. 1(d). The plot reveals a linear elastic response up to the yield point, which is observed at a critical strain of ~ 0.055 . Here, τ_{max} reaches a value of ~ 7.5 GPa, which is a substantial fraction of the theoretical shear strength τ_{th} of tantalum ($G/2\pi \sim 11$ GPa, where G is the shear modulus of Ta, 69 GPa), as it would be expected for the process of homogeneous dislocation nucleation. As a reference, the star

symbol in Fig. 1(a) marks the point on the elastic part of the load-displacement curve where condition $\tau_{\max} = \tau_{th}$ would be fulfilled.

The nanoindentation data shown in Fig. 1 seem to be characteristic of (001) oriented bcc single crystals as very similar results have been reported for W and Fe.^{16,18,21} As mentioned above, the observation of a 30 nm displacement excursion within 1 ms requires the existence of extremely efficient dislocation nucleation and multiplication processes. In this context, it is interesting to speculate about the fate of the energy ($\sim 5 \times 10^{-12}$ J, load times displacement, $\sim 200 \mu\text{N} \times 30$ nm), which is released and dumped into the indented material during this process. In the extreme case of an adiabatic scenario, this could lead to a local temperature spike of up to several hundred kelvin depending on the plastic deformation volume.³⁷ Furthermore, the occurrence of only one discontinuity in the P - h curves indicates that the dislocation sources generated during the displacement burst are very stable and able to operate continuously at relatively low stress levels throughout the entire elastic-plastic loading regime.³⁸ Theoretical studies will be necessary to identify the microscopic origin of the rapid dislocation nucleation and multiplication processes during the onset of plasticity in bcc materials.

The observations discussed above are in contrast to the load-displacement behavior typically observed for close-packed metals such as Au,⁸ Ni,³⁴ Pt,³ and Al,²¹ which all show a sequence of very small (few nanometers) displacement excursions (staircaselike loading behavior). That is, the elastic-plastic regime is repeatedly interrupted by elastic loading, indicating exhaustion and regeneration of dislocation sources. It is tempting to attribute this difference to the difference in Peierls stress rather than to the presence of an oxide layer. Ta, as well as other bcc metals, exhibits a high Peierls stress in the order of $0.03G$,³⁹ whereas the Peierls stress of close-packed metals is typically in the order of 10^{-5} to $10^{-6} G$.⁴⁰ This interpretation is consistent with the fact that very similar load-displacement curves have been reported for other high Peierls stress materials such as GaAs (covalent) and CaF₂ (ionic).³⁴ In the case of bcc metals, the high Peierls stress is a consequence of the complicated core structure of screw dislocations. The relative stability of the dislocation sources in Ta (as suggested by the observation of only one excursion) therefore seems to be linked to the sessile (immobile) character of screw dislocations in bcc metals in the low temperature range ($T < 0.15T_{\text{melting}}$).

To assess the influence of surface roughness on the load-displacement behavior, we performed a number of nanoindentation experiments on surfaces roughened by low-dose 2 keV Ar⁺ ion bombardment ($\sim 10^{16}$ Ar⁺/cm²). This treatment creates a nanoscale pit and mound surface morphology with a peak-to-valley roughness of only a few atomic layers⁴¹ and therefore allows one to modify the surface roughness with atomic level control. Note that the native oxide layer reforms immediately during exposure to air. Figure 2 shows two sets of nanoindentation data collected from the same area before and after ion bombardment. It is obvious that pop-ins are completely suppressed by increasing the surface roughness. The elastic loading regime is no longer observed, indicating, that yielding starts at much lower ap-

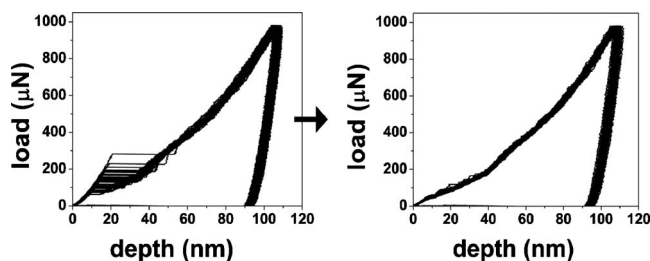


FIG. 2. Effect of surface roughness on the load-displacement behavior of Ta(001): Nanoindentation data collected from the same area before (left) and after (right) ion bombardment. Note that both the initial elastic loading regime and the pop-in events are suppressed by increasing the surface roughness via low-energy ion-bombardment.

plied load levels due to stress concentration at surface asperities. These experiments provide direct evidence for the conclusion of a recent variable-temperature nanoindentation study, namely, that incipient plasticity involves heterogeneous nucleation sites such as vacancies, surface asperities, or preexisting dislocations.^{3,6}

As mentioned above, the nanoindentation curves are very reproducible. Analyzing the load-displacement curves with respect to the critical load necessary to induce plasticity reveals a narrow distribution [Fig. 3(a)]. In view of the surface roughness effect described above, the narrow load distribution shown in Fig. 3(a) reflects the high quality of our surface finish. Indeed, we observe that the distribution broadens upon continuous use of the crystal, indicating that the surface finish deteriorates due to frequent cleaning. As a side note, we do not observe a difference between surfaces obtained by a final electropolishing step and those prepared by mechanical polishing as long as a high-quality surface finish is obtained. We also observe a weak dependence of the loading

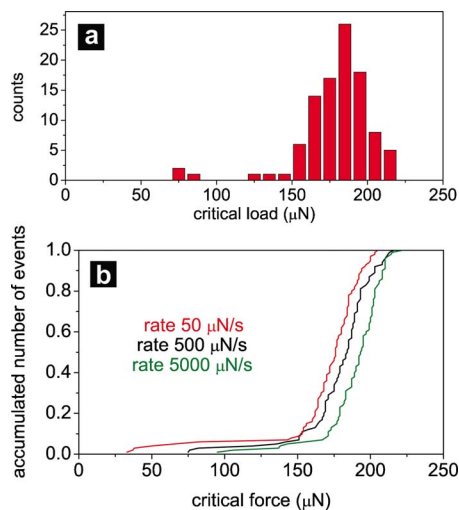


FIG. 3. (Color online) Reproducibility of the experiment and effect of loading rate on the critical load: (a) A narrow distribution of the critical load reveals the homogeneity of the surface finish. (b) The load necessary to induce a pop-in event shifts toward higher loads with increasing loading rate.

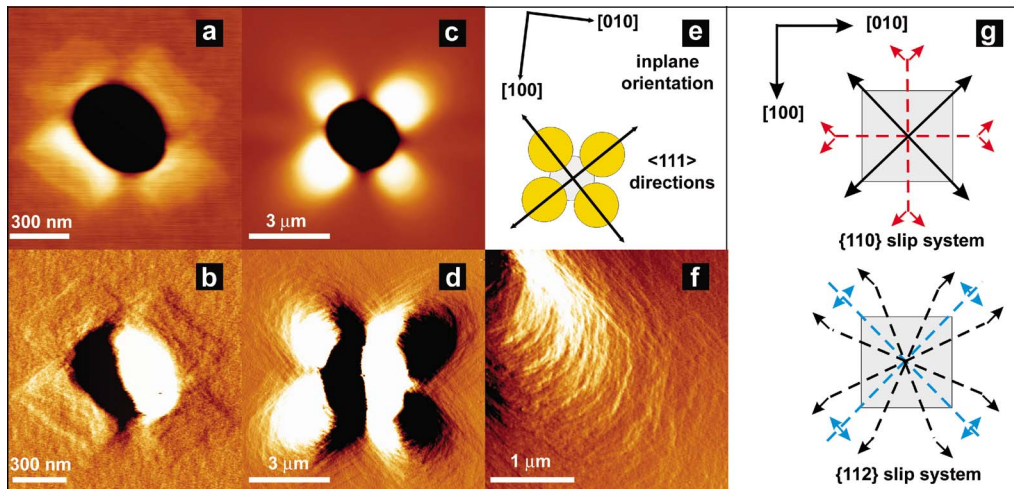


FIG. 4. (Color online) AFM images from indents produced with a spherical tip: topographic (top) as well as deflection mode (bottom) AFM images from a test loaded just above the onset of plasticity [(a) and (b)] as well as of a deeper indent [(c), (d), and (f)]. (e) In-plane surface orientation as obtained by EBSD; (g) orientation of intersections of the slip planes with the $[001]$ surface plane for both the $\{110\}\langle 111 \rangle$ and the $\{112\}\langle 111 \rangle$ slip system. Note that the majority of the slip lines in the AFM images are consistent with the activation of the $\{110\}\langle 111 \rangle$ slip system.

rate on the onset of plasticity. Following the approach described by Mason *et al.*,³ Fig. 3(b) shows the normalized cumulative distribution of the critical load for three different loading rates ranging from 50 to 5000 μN . Each data set consists of at least 100 individual experiments. The shift of the onset of plasticity toward higher loads with increasing loading rate is consistent with the stress-biased thermally activated dislocation nucleation process postulated by Mason *et al.*³ However, the rate dependence observed in the present study is less pronounced than the one reported for fcc Pt(110) at room temperature,³ which indicates that the stress term is more dominant in the case of bcc metals.

B. Atomic force microscopy

To study the material flow under the indenter and to determine the activated slip system, we performed additional experiments with a spherical indenter. Figure 4 shows AFM images of a shallow indent (just after the occurrence of a pop-in event) as well as of a deeper indent. Independent of the indent depth, we observe a pileup formation, and the symmetry of the pileup pattern reflects the symmetry of the crystal. Specifically, we observe a maximum pileup along the $\langle 111 \rangle$ directions consistent with the $\langle 111 \rangle$ slip directions of a bcc crystal. Slip lines are always very fine and exhibit a wavy appearance [Figs. 4(b) and 4(f)], which is a typical feature of bcc metals and is generally attributed to multiple cross slips of screw dislocations (again, a consequence of the complicated core structure of screw dislocations in bcc metals). Straight segments of slip lines [Figs. 4(b) and 4(f)] seem to be preferentially aligned along the intersections of the (110) and (1 $\bar{1}$ 0) slip planes with the (001) surface plane [Fig. 4(g)]. This suggests that the $\{110\}\langle 111 \rangle$ slip system is preferred over the $\{112\}\langle 111 \rangle$ slip system, consistent with recent experimental findings.²⁴ In view of attributing pop-in events to dislocation nucleation, it is important to note that we ob-

serve both pileup and slip lines as soon as we observe a residual impression, which is immediately after the occurrence of a pop-in event. The appearance of slip lines requires that the native Ta oxide film supposes no barrier for dislocations and fails via shear at slip edges.⁴² Consistent with our observation, the 1-nm-thick native Ta oxide film is not expected to be a barrier for dislocations due to its thinness and the fact that Young's modulus of Ta oxide (140 GPa) (Ref. 43) is lower than that of Ta (189 GPa).

A closer inspection of the pileup reveals that slip lines are typically 2–3 nm in height, indicating that approximately ten dislocations contribute to each slip line. Thus, the appearance of slip lines reveals highly localized plastic deformation. This is consistent with the proposed stability of the dislocation sources created during the pop-in event: dislocation sources are stable enough to emit numerous dislocations lying in the same lattice plane. Furthermore, in none of the images do we observe evidence for oxide rupture, such as the microcracks reported for W.¹⁶

To study the effect of crystal orientation on material flow under the indenter, we performed additional experiments on Ta(110) and Ta(111) single crystals (Fig. 5). As for the (001) orientation, the pileup pattern reflects the symmetry of the surface (twofold for the (110) and threefold for the (111) surface orientation), with the maximum pileup along the $\langle 111 \rangle$ easy slip directions of the bcc system. It is interesting to note that in the case of the (110) orientation, where both in-plane and out-of-plane slip directions are available, the pileup is predominantly found along the in-plane slip directions. Concerning the corresponding load-displacement curves, we noticed that the single pop-in behavior characteristic for the (001) orientation is less pronounced for (110) and (111) crystals where multiple pop-ins were frequently observed. This orientation dependence cannot be caused by differences in the native oxide film as x-ray photoemission spectroscopy (XPS) reveals the presence of only a

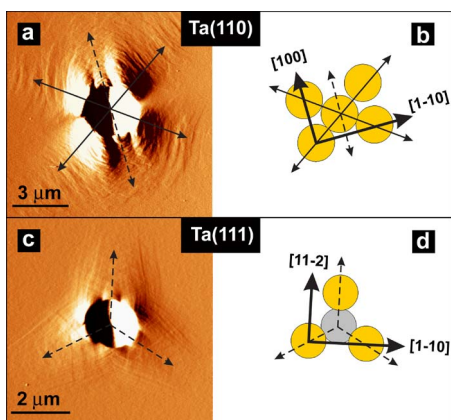


FIG. 5. (Color online) Deflection mode AFM images from spherical indents on (a) Ta(110) and (c) Ta(111) single crystals. The corresponding in-plane surface orientations as well as the in-plane (solid) and out-of-plane (dashed) $\langle 111 \rangle$ slip directions are displayed in (b) and (d). The maximum pileup is always observed along the $\langle 111 \rangle$ slip directions of the bcc crystal structure.

1-nm-thick oxide film on all three surface orientations. Furthermore, this orientation dependence seems to be a general trend for bcc materials since a similar behavior [i.e., pro-

nounced single pop-in behavior of the (001) orientation versus staircaselike load-displacement curves for the (111) orientation] has also been observed for tungsten.¹⁶

IV. CONCLUSION

In summary, our experiments provide strong evidence that the pop-in events observed during nanoindentation experiments on bcc metals coated with a 1-nm-thick oxide layer (such as Ta) are caused by dislocation nucleation rather than by an oxide rupture. Additionally, we have shown that incipient plasticity in Ta involves heterogeneous nucleation sites such as surface asperities, as demonstrated by low-dose ion bombardment experiments. As a final note, we observed by nanoindentation that there are relatively stable dislocation sources in Ta which can be attributed to the sessile character of screw dislocations at the low temperature range.

ACKNOWLEDGMENTS

Work at LLNL was performed under the auspices of the U.S. DOE by the University of California, LLNL under Contract No. W-7405-Eng-48. The authors thank Cheryl L. Evans and Bassem S. El-Dasher for XPS and EBSD characterizations.

*Author to whom correspondence should be addressed; biener2@llnl.gov

- ¹O. Rodriguez de la Fuente, J. A. Zimmerman, M. A. Gonzalez, J. de la Figuera, J. C. Hamilton, W. W. Pai, and J. M. Rojo, *Phys. Rev. Lett.* **88**, 036101 (2002).
- ²E. Carrasco, M. A. Gonzalez, O. Rodriguez de la Fuente, and J. M. Rojo, *Surf. Sci.* **572**, 467 (2004).
- ³J. K. Mason, A. C. Lund, and C. A. Schuh, *Phys. Rev. B* **73**, 054102 (2006).
- ⁴C. A. Schuh, *Mater. Today* **9**, 32 (2006).
- ⁵J. Li, K. J. Van Vliet, T. Zhu, S. Yip, and S. Suresh, *Nature (London)* **418**, 307 (2002).
- ⁶C. A. Schuh, J. K. Mason, and A. C. Lund, *Nat. Mater.* **4**, 617 (2005).
- ⁷A. M. Minor, S. A. S. Asif, Z. W. Shan, E. A. Stach, E. Cyranowski, T. J. Wyrobek, and O. L. Warren, *Nat. Mater.* **5**, 697 (2006).
- ⁸S. G. Corcoran, R. J. Colton, E. T. Lilleodden, and W. W. Gerberich, *Phys. Rev. B* **55**, R16057 (1997).
- ⁹A. Asenjo, M. Jaafar, E. Carrasco, and J. M. Rojo, *Phys. Rev. B* **73**, 075431 (2006).
- ¹⁰J. W. Christian, *Metall. Trans. A* **14A**, 1237 (1983).
- ¹¹M. S. Duesbery and V. Vitek, *Acta Mater.* **46**, 1481 (1998).
- ¹²B. Šesták, *Czech. J. Phys., Sect. B* **22**, 270 (1972).
- ¹³L. P. Kubin, B. Devincre, and M. Tang, *J. Comput.-Aided Mater. Des.* **5**, 31 (1998).
- ¹⁴B. Šesták, *Mater. Sci. Eng.* **25**, 171 (1976).
- ¹⁵D. E. Kramer, K. B. Yoder, and W. W. Gerberich, *Philos. Mag. A* **81**, 2033 (2001).
- ¹⁶D. F. Bahr, D. E. Kramer, and W. W. Gerberich, *Acta Mater.* **46**,

3605 (1998).

- ¹⁷R. Smith, D. Christopher, S. D. Kenny, A. Richter, and B. Wolf, *Phys. Rev. B* **67**, 245405 (2003).
- ¹⁸W. W. Gerberich, J. C. Nelson, E. T. Lilleodden, P. Anderson, and J. T. Wyrobek, *Acta Mater.* **44**, 3585 (1996).
- ¹⁹S. A. S. Asif and J. B. Pethica, *Philos. Mag. A* **76**, 1105 (1997).
- ²⁰N. A. Stelmashenko, M. G. Walls, L. M. Brown, and Y. V. Milman, *Acta Metall. Mater.* **41**, 2855 (1993).
- ²¹K. Durst, B. Backes, O. Franke, and M. Goken, *Acta Mater.* **54**, 2547 (2006).
- ²²W. W. Gerberich, W. M. Mook, M. D. Chambers, M. J. Cordill, C. R. Perrey, C. B. Carter, R. E. Miller, W. A. Curtin, R. Mukherjee, and S. L. Girshick, *J. Appl. Mech.* **73**, 327 (2006).
- ²³H. J. Mathieu, M. Datta, and D. Landolt, *J. Vac. Sci. Technol. A* **3**, 331 (1985).
- ²⁴P. J. Maudlin, J. F. Bingert, and G. T. Gray, *Int. J. Plast.* **19**, 483 (2003).
- ²⁵K. G. Hoge and A. K. Mukherjee, *J. Mater. Sci.* **12**, 1666 (1977).
- ²⁶D. P. Ferriss, R. M. Rose, and J. Wulff, *Trans. Metall. Soc. AIME* **224**, 975 (1962).
- ²⁷R. Lachenmann and H. Schultz, *Z. Metallkd.* **66**, 443 (1975).
- ²⁸B. L. Mordike, *Z. Metallkd.* **53**, 586 (1962).
- ²⁹A. S. Khan and R. Q. Liang, *Int. J. Plast.* **15**, 1089 (1999).
- ³⁰The authors want to emphasize that their experiment cannot completely rule out that a few dislocations nucleate prior to the observation of a pop-in, as previously observed by *in situ* TEM nanoindentation studies (Ref. 7).
- ³¹A. C. Fischer-Cripps, *Nanoindentation* (Springer-Verlag, New York, 2002).
- ³²W. D. Nix and H. J. Gao, *J. Mech. Phys. Solids* **46**, 411 (1998).

- ³³X. Qiu, Y. Huang, W. D. Nix, K. C. Hwang, and H. Gao, *Acta Mater.* **49**, 3949 (2001).
- ³⁴P. Grau, D. Lorenz, and A. Zeckzer, *Radiat. Eff. Defects Solids* **157**, 863 (2002).
- ³⁵E. G. Herbert, G. M. Pharr, W. C. Oliver, B. N. Lucas, and J. L. Hay, *Thin Solid Films* **398**, 331 (2001).
- ³⁶S. Basu, A. Moseson, and M. W. Barsoum, *J. Mater. Res.* **21**, 2628 (2006).
- ³⁷Assuming that the radius of the plastic zone is twice the contact radius results in a local temperature increase of ~ 200 K.
- ³⁸The authors want to note that a staircaselike yielding was previously observed on W(111) and linked to the limited number of slip systems available in this particular orientation (Ref. 16).
- ³⁹G. F. Wang, A. Strachan, T. Cagin, and W. A. Goddard, *Mater. Sci. Eng., A* **309**, 133 (2001).
- ⁴⁰D. Hull and D. J. Bacon, *Introduction to Dislocations* (Butterworth-Heinemann, Oxford, 2001).
- ⁴¹J. Biener, M. M. Biener, T. Nowitzki, A. V. Hamza, C. M. Friend, V. Zielasek, and M. Baumer, *ChemPhysChem* **7**, 1906 (2006).
- ⁴²Y. H. Choo and O. F. Devereux, *J. Electrochem. Soc.* **123**, 1868 (1976).
- ⁴³K. Yamamoto, S. Miyoki, T. Uchiyama, H. Ishitsuka, M. Ohashi, K. Kuroda, T. Tomaru, N. Sato, T. Suzuki, T. Haruyama, A. Yamamoto, T. Shintomi, K. Numata, K. Waseda, K. Ito, and K. Watanabe, *Phys. Rev. D* **74**, 022002 (2006).